Appendix to

SUPERCONDUCTING COPLANAR DELAY LINES

by

YI WANG

A thesis submitted to
The University of Birmingham
for the degree of
DOCTOR OF PHILOSOPHY

Electronic, Electrical and Computer Engineering
School of Engineering
The University of Birmingham
February 2005

Appendix A Loss in coplanar waveguides

The main task of this section is to develop an analytical expression for the conductor loss of a CBCPW line, in order to evaluate the loss increment due to the presence of conductor backing. The derivation is based on the incremental-inductance method. For completeness, the derivation with a CPW line is also presented, which results in the same expression as given by Gupta[1]. To begin with, the analytical models to calculate the dielectric loss and conductor loss are reviewed. Besides the incremental-inductance method, a current-distribution method is also introduced. It should be noted that both methods are originally established for normal conductors. For superconductors, some corrections are needed in using these analytical methods, which have been mentioned in the text of Chapter 4.

A.1 Introduction

For a wave propagating in the z direction, the transmitted power in terms of attenuation coefficient α can be expressed as

$$P(z) = P_0 e^{-2\cdot\alpha\cdot z}$$

where P_0 is the transmitted power at z=0. The attenuation mainly results from the conductor loss α_c and the dielectric loss α_d. That is

$$\alpha = \alpha_c + \alpha_d .$$

This can be expressed in terms of the power dissipation per unit length of conductors (P_c) and dielectrics (P_d).

$$\alpha = -\frac{dP(z)/dz}{2P(z)} \approx \frac{P_c + P_d}{2P(z)}$$

(α is in nepers per unit length.) So,

$$\alpha_c = \frac{P_c}{2P(z)} \text{ and } \alpha_d = \frac{P_d}{2P(z)},$$

or, in dB per unit length

$$\alpha_c = \frac{20}{\ln(10)}\frac{P_c}{2P(z)} = 8.686\frac{P_c}{2P(z)} \text{ and } \alpha_d = 8.686\frac{P_d}{2P(z)}.$$

Sometimes, the attenuation is in units of nepers per wavelength rather than the physical length in order to include the effect of effective permittivity.

A.2 Dielectric Loss

The loss tangent of a dielectric medium is defined as

$$\tan\delta = \frac{\omega\varepsilon'' + \sigma}{\omega\varepsilon'} = \frac{\sigma_e}{\omega\varepsilon'}$$

ε'' and ε' are the imaginary part and real part of the permittivity of the dielectric. The total effective conductivity σ_e includes two parts: the dielectric damping $\omega\varepsilon''$ and the finite conductivity of the dielectric medium σ.

For a transmission line with uniform medium, the attenuation due to the dielectric is (pp. 85-86 in [1])

$$\alpha_{du} = \frac{g'Z_0}{2} = \frac{\sigma_e\sqrt{\mu/\varepsilon'}}{2} = \frac{\omega\sqrt{\mu\varepsilon'}}{2}\tan\delta$$

where g' is the shunt conductance per unit length of the transmission line. When the dielectric medium is not uniform, an effective loss tangent $(\tan\delta)_{eff}$ can be introduced.

$$\alpha_d = \frac{\omega\sqrt{\mu\varepsilon_{eff}\varepsilon_0}}{2}(\tan\delta)_{eff}$$

As the conductivity of air σ_0 is much smaller than that of the dielectric,

$$\sigma_e = q\sigma + (1-q)\sigma_0 \approx q\sigma$$

where q is the dielectric filling fraction. Also

$$\varepsilon_{eff}\varepsilon_0 = q\varepsilon_r\varepsilon_0 + (1-q)\cdot\varepsilon_0 .$$

In both cases,

$$q = \frac{\varepsilon_{eff}-1}{\varepsilon_r - 1} .$$

Hence, the dielectric attenuation coefficient can be derived.

$$\alpha_d = \frac{\omega\sqrt{\mu(\varepsilon_{eff}\varepsilon_0)}}{2}\frac{q\sigma}{\omega(\varepsilon_{eff}\varepsilon_0)} = q\sqrt{\frac{\varepsilon_r}{\varepsilon_{eff}}}\left(\frac{\omega\sqrt{\mu(\varepsilon_r\varepsilon_0)}}{2}\frac{\sigma}{\omega(\varepsilon_r\varepsilon_0)}\right)$$

$$= q\sqrt{\frac{\varepsilon_r}{\varepsilon_{eff}}}\left(\frac{\omega\sqrt{\mu(\varepsilon_r\varepsilon_0)}}{2}\tan\delta\right) = \pi\sqrt{\mu\varepsilon_0}\frac{\varepsilon_{eff}-1}{\varepsilon_r-1}\frac{\varepsilon_r}{\sqrt{\varepsilon_{eff}}}\tan\delta\cdot f$$

$$= \frac{\pi}{c_0}\frac{\varepsilon_{eff}-1}{\varepsilon_r-1}\frac{\varepsilon_r}{\sqrt{\varepsilon_{eff}}}\tan\delta\cdot f$$

A.3 Conductor loss

A.3.1 Current density distribution method

If the current distribution in the conductors is known, one can find the ohmic power loss by an integration, and the attenuation can be expressed as[2]

$$\alpha_c = \frac{R_f}{2Z_0}\frac{\oint_\gamma |J|^2 dl}{I^2}$$

where I is the total current carried by the transmission line, J the longitudinal current density on the line, and γ is the contour of the conductors for the integration. R_f is the surface resistance. Z_0 is the characteristic impedance. The current density distribution is not uniform and peaks at the edges of the conductors. It can be obtained either analytically by conformal mapping or numerically. Here, only analytical methods are summarised.

Ghione[3] did extensive studies on the loss of asymmetric coplanar waveguide (ACPW) based on conformal mapping, which was originally presented by Owyang[4]. To find the current distribution, conductors with finite thickness have to be dealt with. This involves two mappings. First, the upper half of the original structure (ζ-plane) with finite thickness conductors is transformed via $z(\zeta)$ into the upper half z-plane with infinitely thin conductors. Then the resultant z-plane structure is transformed via $w(z)$ into the interior of a rectangle in w-plane. Following a reversed process of the two-step mapping, the current density in the original structure can be expressed by the uniform current density $\tilde{I}^{ACPS}$ in the w-plane and two scale factors $|dw/dz|$ and $|dz/d\zeta|$ as

$$J(\zeta) = \tilde{I}^{ACPS}\left|\frac{dw}{dz}\right| \cdot \left|\frac{dz}{d\zeta}\right|$$

The detailed deviations are available in the work by Owyang and Ghione. As the symmetric version of Ghione's general formula for ACPW, the attenuation of a CPW can be given by

$$\alpha_c^{CPW} = \frac{8.68R_f}{16Z_0K^2(k)\left[1-(a/b)^2\right]}\left\{\frac{2}{a}\left[\pi + \ln\left[4\pi\frac{a(b-a)}{t(b+a)}\right]\right] + \frac{2}{b}\left[\pi + \ln\left[4\pi\frac{b(b-a)}{t(b+a)}\right]\right]\right\}$$

(Note: There is an error or misprint in Owyang's (21)[4] by a factor 2. The right expression is (21) divided by 2, which is Ghione's (45)[3]. In addition, the "t" in Owyang's formulas is half of the conductor thickness. In this thesis, "t" denotes the conductor thickness. The "a" and "b" used in this thesis is twice the ones used in Owyang's and Ghione's work.)

A.3.2 Incremental inductance method

If the current distribution is difficult to obtain, one can use another technique, the "incremental inductance rule" to derive the conductor loss, first published in 1942 by Wheeler[5] and developed by Pucel[6]. In Wheeler's method, the surface resistance per unit length caused by the

skin effect is expressed in terms of the inductance produced by the magnetic field within the conductor. Therefore, the accuracy of this method very much depends on the accuracy of the inductance. The formulation is based on the fact that the series surface impedance of the conductor

$$Z_s = R + jX$$

has a real part R which equals to its imaginary part X, that is*

$$R = X = \omega L_i ,$$

where L_i is the internal inductance caused by a thin layer of current flow due to the skin effect. According to the "incremental inductance rule", L_i can be derived as an increment of the external inductance L due to the incremental recessions of all conductive walls by half of the skin depth. This rule assumes that the radius of the curvatures and the thickness of the conductors exposed to the electromagnetic field are larger than the skin depth, preferably several skin depths. The internal inductance can be expressed as

$$L_i = \sum_m \frac{\mu_m}{\mu_0} \frac{\partial L}{\partial n_m} \frac{\delta_m}{2}$$

Hence, the resistance is

$$R = \frac{1}{\mu_0} \sum_m R_{s,m} \frac{\partial L}{\partial n_m} ,$$

where $R_{s,m} = \omega \mu_m \delta_m / 2$ is the surface resistance of the conductor wall m. The attenuation coefficient can be derived as

$$\alpha_c = \frac{P_c}{2P(z)} = \frac{I^2 R}{2I^2 Z_0} = \frac{1}{2\mu_0 Z_0} \sum_m R_{s,m} \frac{\partial L}{\partial n_m}$$

The external inductance L can be related to the characteristic impedance of the transmission line with the dielectric replaced by air. i.e.

$$L = Z_0^a / c_0$$

where c_0 is the velocity of the electromagnetic wave in free space.

The conductor losses of both CPW and CBCPW will be derived using the incremental inductance method.

* This relation is not true for superconductors. As discussed in Section 3.2.4, the surface impedance of a superconductor is expressed as

$$Z_s = R_s + jX_s \approx \sqrt{\frac{\omega\mu}{\sigma_2}} \left(\frac{\sigma_1}{2\sigma_2} + j \right).$$

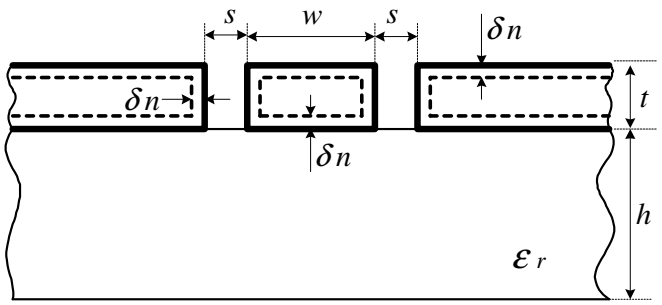

Figure A.1 Recession of the conductors of CPW for loss calculation using incremental inductance method.

A.3.2.1 Conductor loss of CPW

As illustrated in Figure A.1, the recessions of the conductor surfaces in CPW are

$\partial w = -2\partial n$ (due to the recession of either edge of the strip),

$\partial s = 2\partial n$ (due to the recession of one edge of the strip and one of the in-plane grounds),

$\partial t = -2\partial n$ (due to the recession of the top and bottom of the conductors).

The attenuation due to conductor loss can be expressed as

$$\alpha_c^{CPW} = \frac{8.68}{\mu_0 c_0 Z_0^{CPW}} R_f^s \left(\frac{\partial Z_0^a}{\partial s} - \frac{\partial Z_0^a}{\partial w} - \frac{\partial Z_0^a}{\partial t} \right)$$

To calculate the attenuation using the above formula, one must know the effect of conductor thickness t on the characteristic impedance. This effect is taken into account by correcting the line width and slot width with[1]

$$\Delta = 1.25 \frac{t}{\pi} \left(1 + \ln \left(\frac{4\pi w}{t} \right) \right).$$

This gives the effective line width and the effective slot width,

$$w_e = w + \Delta \,,\; s_e = s - \Delta \,.$$

Let

$$k_1 = w_e / (w_e + 2s_e)$$

$$P = \begin{cases} \dfrac{k_1}{\left(1 - \sqrt{1 - k_1^2}\right)\left(1 - k_1^2\right)^{0.75}} & if \quad 0 \le k_1 \le 0.707 \\ \dfrac{1}{(1 - k_1)\sqrt{k_1}} \left(\dfrac{K\left(\sqrt{1 - k_1^2}\right)}{K(k_1)} \right)^2 & if \quad 0.707 < k_1 \le 1 \end{cases}$$

$$P' = \left(\frac{K(k_1)}{K\left(\sqrt{1-k_1^2}\right)} \right)^2 P$$

The final expression of the attenuation coefficient of CPW can be written as[1]

$$\alpha_c^{CPW} = \frac{8.68 \cdot R_f Z_0 \varepsilon_{eff}}{15\pi^2 \mu_0 c_0} \frac{P'}{s}\left(1+\frac{w}{s}\right) \frac{1+\frac{1.25t}{\pi w}+\frac{1.25}{\pi}\ln\left(\frac{4\pi w}{t}\right)}{\left(2+\frac{w}{s}-\frac{1.25t}{\pi s}\left(1+\ln\left(\frac{4\pi w}{t}\right)\right)\right)^2}.$$

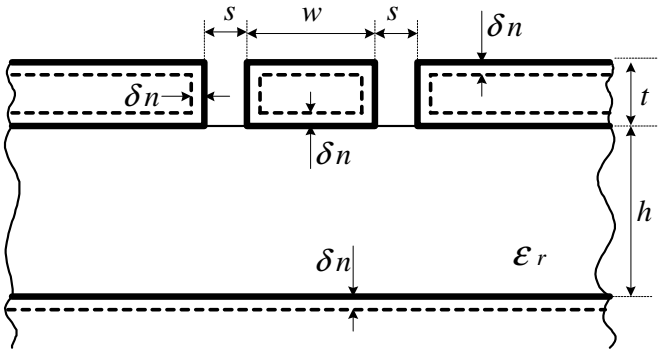

Figure A.2 Recession of the conductors of CBCPW for loss calculation using incremental inductance method.

A.3.2.2 Loss of CBCPW

There have not been any formulations of the loss for CBCPW in the literature. In order to find the loss increment due to the conductor backing, analytical expressions are developed here based on the incremental-inductance method. As illustrated in Figure A.2, the recessions of the conductor surfaces considered in CBCPW are

$\partial w = -2\partial n$ (due to the recession of either edge of the strip),

$\partial s = 2\partial n$ (due to the recession of one edge of the strip and one of the in-plane grounds),

$\partial t = -2\partial n$ (due to the recession of the top and bottom of the conductors),

$\partial h = \partial n$ (due to the recession of the bottom of the conductors),

$\partial h = \partial n$ (due to the recession of the conductor backing).

As pointed out in [6] when dealing with the ground of the microstrip, it is "on somewhat uncertain ground, however, in deciding whether the recession of the bottom surface of the strip conductor can be counted towards a recession in t as well as an extension of h". It is assumed so here for the coplanar waveguide as was for microstrip in [6], where a larger value of α_c was obtained and agrees better with the measured results.

The attenuation of the CBCPW can be expressed as

$$\alpha_c^{CBCPW} = \frac{8.68}{\mu_0 c_0 Z_0^{CBCPW}} \left[R_f^s \left(\frac{\partial Z_0^a}{\partial s} - \frac{\partial Z_0^a}{\partial w} - \frac{\partial Z_0^a}{\partial t} + \frac{1}{2}\frac{\partial Z_0^a}{\partial h} \right) + R_f^g \left(\frac{1}{2}\frac{\partial Z_0^a}{\partial h} \right) \right]$$

where R_f^s and R_f^g are the surface resistances on the strip and the conductor-backing. Assume $R_f^s = R_f^g$.

I. Narrow coplanar line with *h*>>*w* and *h*>>*s*

For the CBCPW used in this work, as the substrate thickness h is much larger than the strip width w and slot width s, the conductor backing has little effect on the fringe field of the coplanar conductors. Therefore, the similar correction can be adopted for CBCPW as for the conventional CPW in [1]. The effective strip and slot widths are defined as

$$w_e = w + 1.25\frac{t}{\pi}\left[1 + \ln\left(\frac{4\pi w}{t}\right)\right],\ s_e = s - 1.25\frac{t}{\pi}\left[1 + \ln\left(\frac{4\pi w}{t}\right)\right],\ h_e = h.$$

Let

$$k_1 = w_e/(w_e + 2s_e), \qquad k_2 = A/B$$

where

$$A = \tanh\left(\frac{\pi w_e}{4h}\right), \qquad B = \tanh\left[\frac{\pi(w_e + 2s_e)}{4h}\right]$$

and

$$X_{i,i=1,2} = \begin{cases} \left[\dfrac{K(k_i)}{K\left(\sqrt{1-k_i^2}\right)}\right]^2 \dfrac{k_i}{\left(1-\sqrt{1-k_i^2}\right)\left(1-k_i^2\right)^{0.75}}, & 0 \le k_i \le 0.707, \\ \dfrac{1}{(1-k_i)\sqrt{k_i}}, & 0.707 < k_i \le 1. \end{cases}$$

$$Y_1 = \frac{2(w_e + s_e)}{(w_e + 2s_e)^2}\left[1 + \frac{1.25t}{\pi w} + \frac{1.25}{\pi}\ln\left(\frac{4\pi w}{t}\right)\right]$$

$$Y_2 = \frac{(B-A)(1+AB) + 2A}{B^2}\left[\frac{\pi}{4h} + \frac{1.25t}{4hw} + \frac{1.25}{4h}\ln\left(\frac{4\pi w}{t}\right)\right] - \frac{A(1-B^2)}{B^2}\frac{\pi s_e}{2h^2} + \frac{(B-A)(1+AB)}{B^2}\frac{\pi w_e}{4h^2}$$

The attenuation coefficient of the CBCPW due to conductor loss can be expressed as

$$\alpha_c^{CBCPW} = \frac{8.68}{60\pi^2 \mu_0 c_0} R_f \varepsilon_{eff} Z_0^{CBCPW} \left(X_1 \cdot Y_1 + X_2 \cdot Y_2\right)$$

When the substrate is sufficiently thick, this attenuation approaches the one predicted for a

CPW, as expected.

II. Wide coplanar line with *w* comparable to or larger than *h*

When *w* is comparable or larger than *h*, the fringe field will be greatly affected by the presence of the conductor-backing. The aforementioned correction, only depending on *w* and *t*, may not be valid. A correction depending on *h* and *t* can be used, which was mentioned in [7].

$$\Delta' = \frac{1.25t}{\pi}\left(1+\ln\left(\frac{2h}{t}\right)\right)$$

$$w_e = w+\Delta',\ s_e = s-\Delta',\ h_e = h$$

Again let

$$k_1 = w_e/(w_e+2s_e),\qquad k_2 = A/B$$

$$A = \tanh\left(\frac{\pi w_e}{4h_e}\right),\ B = \tanh\left(\frac{\pi(w_e+2s_e)}{4h_e}\right),$$

$$X_i'(i=1,2) = \begin{cases}\left(\dfrac{K(k_i)}{K\left(\sqrt{1-k_i^2}\right)}\right)^2 \dfrac{k_i}{\left(1-\sqrt{1-k_i^2}\right)\left(1-k_i^2\right)^{0.75}} & if \quad 0\le k_i\le 0.707\\ \dfrac{1}{(1-k_i)\sqrt{k_i}} & if \quad 0.707 < k_i \le 1\end{cases}$$

$$Y_1' = \frac{2(s_e+w_e)}{(w_e+2s_e)^2}\left(1+\frac{1.25}{\pi}\ln\left(\frac{2h}{t}\right)-\frac{1.25t}{\pi h}\right)$$

$$Y_2' = \frac{(B-A)(1+A\cdot B)}{B^2}\left(\frac{\pi}{4h}-\frac{\pi}{4h^2}\left(\frac{1.25t}{\pi}-w_e\right)+\frac{1.25}{4h}\ln\left(\frac{2h}{t}\right)\right)$$
$$+\frac{A}{B^2}\left(\frac{\pi}{2h}+\frac{1.25}{2h}\ln\left(\frac{2h}{t}\right)-\frac{\pi}{2h^2}\left(\frac{1.25t}{\pi}+(1-B^2)s_e\right)\right)$$

The attenuation in this case is expressed as

$$\alpha_c^{CBCPW'} = \frac{8.68}{60\pi^2\mu_0 c_0}R_f\varepsilon_{eff}Z_0^{CBCPW}\left(X_1'Y_1'+X_2'Y_2'\right)$$

The problem of this correction (Δ') is its divergence with increasing substrate thickness *h*. This also results in a divergent attenuation, which is physically unreasonable. So the valid range of this correction is restricted. It is believed that this correction is only usable when *h* is comparable or smaller than *w*. In addition, according to [8], this correction overestimates the characteristic impedance.

It is worth mentioning that the two corrections Δ and Δ' were first reported in [9] to consider the effect of conductor thickness on the characteristic impedance of a microstrip line, where the effective line width is

$$w_e = \begin{cases} w + 1.25\frac{t}{\pi}\left[1 + \ln\left(\frac{4\pi w}{t}\right)\right], & w/h \le 1/2\pi, \\ w + 1.25\frac{t}{\pi}\left[1 + \ln\left(\frac{2h}{t}\right)\right], & w/h \ge 1/2\pi. \end{cases}$$

The first expression is for narrow microstrip line, while the second is for relatively wider one with $w/h \ge 1/2\pi$.

[1] K. C. Gupta, R. Garg, I. Bahl, P. Bhartia, *Microstrip lines and slotlines*, 2nd ed., Artech House, 1996
[2] R. E. Collin, *Field theory of guided waves*, McGraw-Hill, pp. 124-128, 1960.
[3] G. Ghione, "A CAD-oriented analytical model for the losses of general asymmetric coplanar lines in hybrid and monolithic MICs", *IEEE Trans. Microwave Theory Tech.*, vol. 41, no. 9, pp. 1499-1510, Sep. 1993.
[4] G. H. Owyang, T. T. Wu, "The approximate parameters of slot lines and their complement", *IRE Trans. Anten. Propag.*, pp. 49-55, Jan. 1958.
[5] H. A. Wheeler, Formulas for the skin effect, *Proceedings of the I.R.E.*, pp. 412-424, Sept. 1942.
[6] R. A. Pucel, D. J. Massé, C. P. Hartwig, "Losses in microstrip", *IEEE Trans. Microwave Theory Tech.*, vol. 16, no. 6, pp. 342-350, Jun. 1968.
[7] Y. C. Shih, M. Maher, "Characterization of conductor-backed coplanar waveguide using accurate on-wafer measurement techniques", in *1990 IEEE MTT-S Int. Microwave Symposium Digest*, pp. 1129-1132, 1990.
[8] R. N. Simons, *Coplanar Waveguide Circuits Components and System*, Wiley-IEEE Press, Apr. 2001.
[9] I. J. Bahl, R. Garg, "Simple and accurate formulas for microstrip with finite strip thickness", *Proc. IEEE*, vol. 65, pp. 1611-1612, 1977.

Appendix B Conformal mapping for coupled coplanar lines

This section presents the conformal-mapping formulas used to calculate the even- and odd-mode impedances of parallel coupled lines. Figure B.1 shows the cross-section of a pair of CBCPW lines with a separation of l_x. Ghione[1] has given some simple formula to evaluate these for CPW lines, assuming an infinite substrate thickness. The formulation adopted here relies on the work by Cheng[2,3] and Zhou[4], which takes the finite substrate thickness into account. Two special functions are used in the following derivation.

(1) Complete elliptic integral of the first kind

$$K(k) = \int_0^1 \frac{1}{\sqrt{(1-w^2)(1-k^2w^2)}}\,dw$$

(2) Incomplete elliptic integral of the first kind

$$F(\phi,k) = \int_0^{\phi} \frac{1}{\sqrt{1-k^2\sin^2(\Phi)}}\,d\Phi$$

$$K(k) = F(\pi/2,k)$$

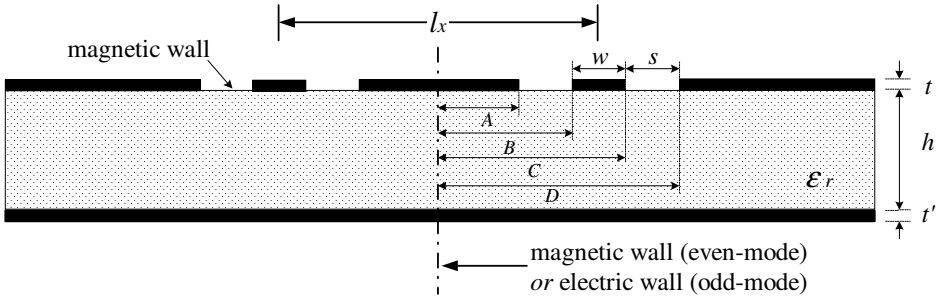

Figure B.1 Dimensional symbols for the coupled CBCPW lines. The coupled CPW lines have similar structure but without the conductor backing. The centre-to-centre separation between the two lines is l_x=B+C.

B.1 Z_e and Z_o of coupled CPW lines

Assuming the air-dielectric interface in the plane with the slots is perfect magnetic wall as shown in Figure B.1, the capacitance of the even- and odd-mode can be considered as a sum of the capacitances in the upper region (air) and lower region (air and dielectric). In the lower region, the capacitance can be further approximated to a sum of the free-space capacitance in absence of the dielectric and the capacitance in the dielectric with a relative permittivity of (ε_r-1). That is

$$C_{e,o} = C_{e,o}^{air(up)} + C_{e,o}^{air+\varepsilon_r(down)} = C_{e,o}^{air(up)} + (C_{e,o}^{air(down)} + C_{e,o}^{\varepsilon_r - 1}) = 2C_{e,o}^{air(up)} + C_{e,o}^{\varepsilon_r - 1} \quad \textbf{Equation B-1}$$

Once the capacitance is obtained, the characteristic impedance can be written as

$$Z_{e,o} = \frac{1}{c_0 \cdot \sqrt{C_{e,o}(\varepsilon_r) \cdot C_{e,o}(1)}} \quad \textbf{Equation B-2}$$

The coupling coefficient is

$$c = \frac{Z_e - Z_o}{Z_e + Z_o}$$

The symmetric plane in Figure B.1 can be regarded as a magnetic wall for the even-mode or an electric wall for the odd-mode. Conformal mapping method is used to calculate the capacitances in (B-1).

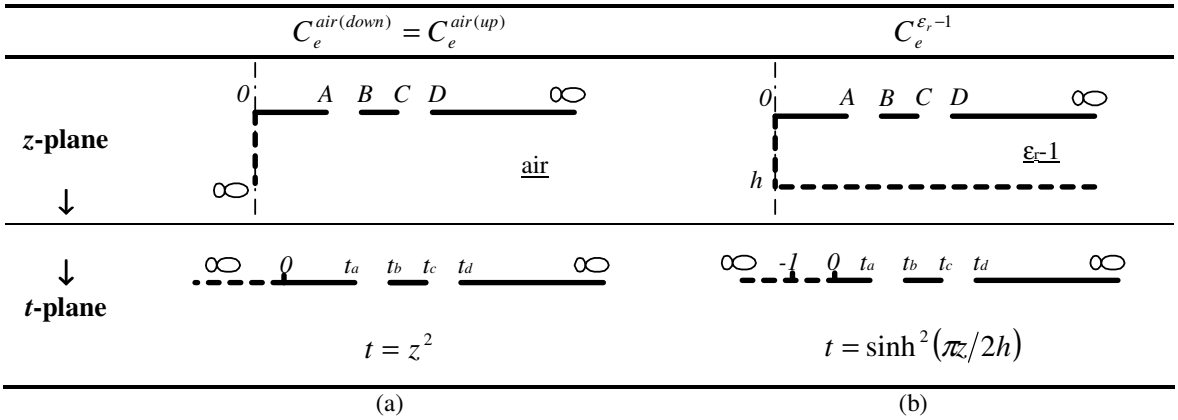

Figure B.2 Conformal mapping for the even-mode of coupled CPW lines: (a) the lower region of free space (infinite thickness); (b) the lower dielectric region with a relative permittivity (ε_r-1) and thickness h.

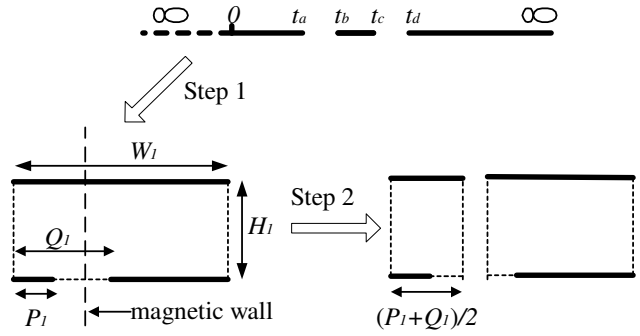

Figure B.3 Conformal mapping from t-plane to rectangular structures for the calculation of the capacitance.

B.1.1 Even mode

As shown in Figure B.2, the original structures with a magnetic wall are in z-plane and then mapped to t-plane. The transformation function $t(z)$ for the lower region of free space

(Figure B.2(a)) is different from that for the dielectric region (Figure B.2(b)). However, the further transformations required to map into rectangular structures are the same for both cases, as shown in Figure B.3. Take the case in Figure B.2(a) as an example. The *z*-plane to *t*-plane transformation gives

$$t_a=A^2,\ t_b=B^2,\ t_c=C^2,\ t_d=D^2,$$

The first mapping step in Figure B.3 can be expressed as

$$k_a = \sqrt{\frac{(t_d - t_a)(t_c - t_b)}{(t_c - t_a)(t_d - t_b)}} \qquad \textbf{Equation B-3(a)}$$

$$\frac{W1}{H1} = \frac{K(k_a)}{K'(k_a)} = \alpha \qquad \textbf{Equation B-3(b)}$$

$$\frac{P1}{W1} = \frac{F(\arcsin(\sqrt{\frac{t_a(t_d-t_b)}{t_b(t_d-t_a)}}), k_a)}{K(k_a)} = \beta 1 \qquad \textbf{Equation B-3(c)}$$

$$\frac{Q1}{W1} = \frac{F(\arcsin(\sqrt{\frac{t_d-t_b}{t_d-t_a}}), k_a)}{K(k_a)} = \beta 2 \qquad \textbf{Equation B-3(d)}$$

$$\beta 3 = (\beta 1 + \beta 2)/2 \qquad \textbf{Equation B-3(e)}$$

For the second mapping step in Figure B.3, a vertical magnetic wall is assumed at the centre of the slot, which is only approximate. The capacitance can be expressed as the contributions from the two separate parts by

$$C_e^{air(up)} = C_e^{air(down)} = \varepsilon_0 \left(\frac{K(k_d)}{K'(k_d)} + \frac{K(k_e)}{K'(k_e)} \right)$$

where k_d and k_e can be found using the following process.

From $\frac{K(k_b)}{K(k_b')} = \alpha \cdot \beta 3$, solve for k_b; **Equation B-3(f)**

from $\frac{K(k_c)}{K(k_c')} = \alpha \cdot (1 - \beta 3)$, solve for k_c; **Equation B-3(g)**

knowing k_b, from $\frac{F(\arcsin(k_d / k_b), k_b)}{K(k_b)} = \frac{\beta 1}{\beta 3}$, solve for k_d; **Equation B-3(h)**

knowing k_c, from $\frac{F(\arcsin(k_e / k_c), k_c)}{K(k_c)} = \frac{1 - \beta 2}{1 - \beta 3}$, solve for k_e. **Equation B-3(i)**

There have been difficulties in solving k_d and k_e using numerical method due to poor convergence. A close-form approximation given in [5] is adapted to find them explicitly.

In the case of Figure B.2(b) for the region of the dielectric, take (ε_r-1) as the relative permittivity and let

$$t_a = \sinh^2\left(\frac{\pi A}{2h}\right),\ t_b = \sinh^2\left(\frac{\pi B}{2h}\right),\ t_c = \sinh^2\left(\frac{\pi C}{2h}\right),\ t_d = \sinh^2\left(\frac{\pi D}{2h}\right).$$

Following the same procedure as Eq. B-3(a)~(i) to solve k_d^* and k_e^*, $C_e^{\varepsilon r\text{-}1}$ in (B-1) becomes

$$C_e^{\varepsilon_r - 1} = \varepsilon_0(\varepsilon_r - 1)\left(\frac{K(k_d^*)}{K'(k_d^*)} + \frac{K(k_e^*)}{K'(k_e^*)}\right)$$

So the capacitance of the even mode is $C_e = 2C_e^{air(up)} + C_e^{\varepsilon_r - 1}$.

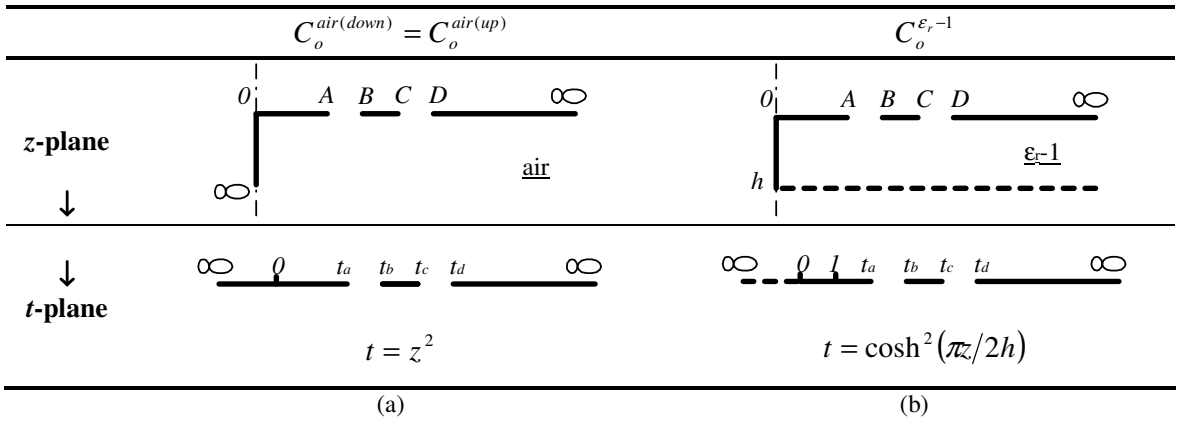

Figure B.4 Conformal mapping for the odd-mode of coupled CPW lines. (a) the lower region in free space (infinite thickness); (b) the lower dielectric region with a relative permittivity (ε_r-1).

B.1.2 Odd mode

For the odd-mode, the symmetric plane is an electric wall as shown in Figure B.4. In the case of Figure B.4(a), the original structure in z-plane is reduced to an asymmetric coplanar waveguide in the t-plane. Therefore, the capacitance $C_o^{air(up)}$ can be simply expressed as

$$C_o^{air(up)} = C_o^{air(down)} = \varepsilon_0\, K(k_a)/K(k_a')$$

In the case of Figure B.4(b), the structure in t-plane is effectively the same as in Figure B.3. So, a similar two-step transformation can be used to find the capacitance. Following the same procedure as to find k_d and k_e in Eq. B-3(a)~(i) and letting

$$t_a = \cosh^2\left(\frac{\pi A}{2h}\right),\ t_b = \cosh^2\left(\frac{\pi B}{2h}\right),\ t_c = \cosh^2\left(\frac{\pi C}{2h}\right),\ t_d = \cosh^2\left(\frac{\pi D}{2h}\right),$$

the capacitance in the dielectric region can be expressed by

$$C_o^{\varepsilon_r-1} = \varepsilon_0(\varepsilon_r - 1)\left[\frac{K(k_d)}{K(k_d')} + \frac{K(k_e)}{K(k_e')}\right]$$

So the capacitance of the odd mode is $C_o = 2C_o^{air(up)} + C_o^{\varepsilon_r-1}$.

B.2 Z_e and Z_o of coupled CBCPW lines

Unlike the CPW, the capacitance of the coupled CBCPW lines can be regarded as the sum of the contributions from the upper region of free space and the lower region of the dielectric with a relative permittivity of ε_r. That is

$$C_{e,o} = C_{e,o}^{air(up)} + C_{e,o}^{\varepsilon_r}$$

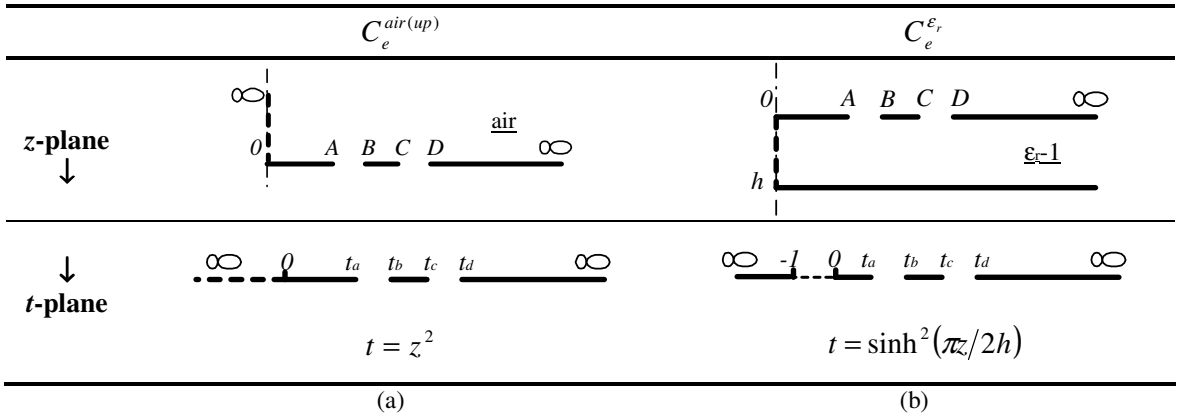

Figure B.5 Conformal mapping for the even-mode of coupled CBCPW lines. (a) the lower region in free space; (b) the lower dielectric region with a relative permittivity ε_r.

B.2.1 Even mode

Figure B.5(a, b) shows the conformal mapping of the even mode. The *t*-planes in both cases can be mapped to rectangular structures as in Figure B.3. In the case of Figure B.5(a), let $t_a=A^2$, $t_b=B^2$, $t_c=C^2$, $t_d=D^2$, and follow Eq. B-3(a)~(i) to solve k_d and k_e. One has

$$C_e^{air(up)} = \frac{K(k_d)}{K(k_d')} + \frac{K(k_e)}{K(k_e')}$$

In the case of Figure B.5(b), repeat the above process with

$$t_a = \sinh^2\left(\frac{\pi A}{2h}\right),\ t_b = \sinh^2\left(\frac{\pi B}{2h}\right),\ t_c = \sinh^2\left(\frac{\pi C}{2h}\right),\ t_d = \sinh^2\left(\frac{\pi D}{2h}\right).$$

but replace Eq. B-3(d) with

$$\frac{Q1}{W1} = \frac{F\left(\arcsin\left(\sqrt{\frac{\cosh^2\left(\frac{\pi A}{2h}\right)}{\cosh^2\left(\frac{\pi B}{2h}\right)}\frac{t_d - t_b}{t_d - t_a}}\right), k_a\right)}{K(k_a)} = \beta 2$$

Substitute the solved k_d and k_e into

$$C_e^{\varepsilon_r} = \frac{K(k_d)}{K(k_d')} + \frac{K(k_e)}{K(k_e')}$$

So, the capacitance of the even mode can be found as

$$C_e = \varepsilon_0 C_e^{air(up)} + \varepsilon_0 \varepsilon_r C_e^{\varepsilon_r}$$

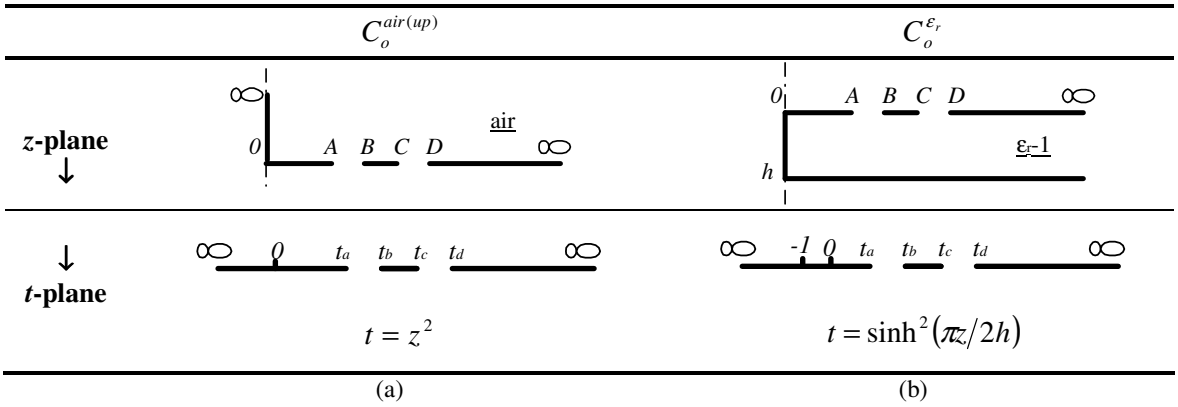

Figure B.6 Conformal mapping for the odd-mode of coupled CBCPW lines: (a) the lower region in free space; (b) the lower dielectric region with a relative permittivity ε_r.

B.2.2 Odd mode

Figure B.6(a, b) shows the conformal mapping of the odd mode. In both cases, the *t*-plane structures can be regarded as asymmetric coplanar waveguides. The capacitance can be expressed as

$$C_o = \varepsilon_0 \frac{K(k_{o1})}{K(k_{o1}')} + \varepsilon_0 \varepsilon_r \frac{K(k_{o2})}{K(k_{o2}')}$$

where

$$k_{o1} = \sqrt{\frac{(D^2 - A^2)(C^2 - B^2)}{(C^2 - A^2)(D^2 - B^2)}}$$

$$k_{o2} = \sqrt{\frac{\left[\sinh^2(\pi D/2h) - \sinh^2(\pi A/2h)\right]\left[\sinh^2(\pi C/2h) - \sinh^2(\pi B/2h)\right]}{\left[\sinh^2(\pi C/2h) - \sinh^2(\pi A/2h)\right]\left[\sinh^2(\pi D/2h) - \sinh^2(\pi B/2h)\right]}}$$

[1] G. Ghione, C. Naldi, "Coplanar waveguides for MMIC applications: effect of upper shielding conductor backing, finite-extent ground planes, and line-to-line coupling", *IEEE Trans. Microwave Theo. Tech.*, vol. 35, no. 3, pp. 260-267, Mar. 1987.

[2] K. K. M. Cheng, "Effect of conductor backing on the line-to-line coupling between parallel coplanar lines", *IEEE Trans. Microwave Theo. Tech.*, vol. 45, no. 7, pp. 1132-1134, 1997.

[3] K. K. M. Cheng, "Analytical formula for calculating the coupling characteristics between parallel coplanar lines", *Electronics Letters*, vol. 32, no. 13, pp. 1208-1209, Jun. 1996.

[4] X. L. Zhou, Y. Wang, S. Wang, "Concise formula of quasistatic parameter for parallel coupling coplanar lines", *Electronics Letters*, vol. 34, no. 17, pp. 1671-1672, 1998.

[5] K. K. M. Cheng, I. D. Robertson, "Quasi-TEM study of microshield lines with practical cavity sidewall profiles", *IEEE Trans. Microwave Theo. Tech.*, vol. 43, no. 12, pp. 2689-2694, 1995.

Appendix C Admittance matrix method

A 2-port 6-node meander line as shown in Figure C.1(a) is taken here as an example to introduce how to construct the admittance matrix and calculate the S parameters.

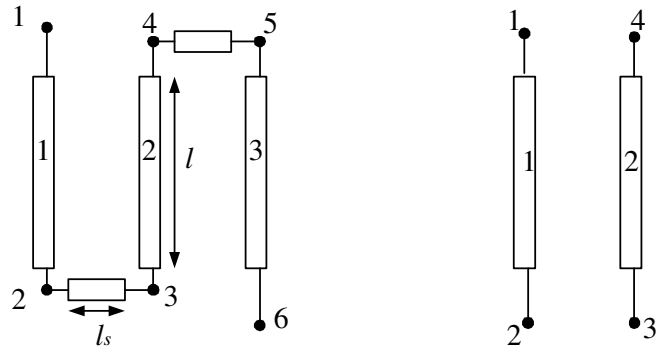

Figure C.1 (a) A 2-port 6-node meander line. *l* is the coupled length and l_s is the length of the connection line. The corners of the bends are disregarded. (b) A pair of coupled lines.

For a pair of coupled lines as shown in Figure C.1(b), there are four independent terms in its admittance matrix: self-admittance Y_1, and transfer-admittances Y_2, Y_3, and Y_4, given by[1]

$$Y_1 = -j\frac{1}{2}\left(Y_e\cot(\theta_e)+Y_o\cot(\theta_o)\right),\quad Y_2 = j\frac{1}{2}\left(Y_e\csc(\theta_e)+Y_o\csc(\theta_o)\right)$$

$$Y_3 = j\frac{1}{2}\left(Y_e\csc(\theta_e)-Y_o\csc(\theta_o)\right),\quad Y_4 = -j\frac{1}{2}\left(Y_e\cot(\theta_e)-Y_o\cot(\theta_o)\right) \qquad \textbf{Equation C-1}$$

where Y_e and Y_o are the even- and odd-mode admittances normalised to the port admittance of $Y_0=1/Z_0=1/(50\Omega)$. The phases are $\theta_e = 2\pi fl/\upsilon_e$, $\theta_o = 2\pi fl/\upsilon_o$ with $\upsilon_e = c_0/\sqrt{\varepsilon_{eff,e}}$, $\upsilon_o = c_0/\sqrt{\varepsilon_{eff,o}}$. The corresponding admittance matrix for the coupled line pair is

$$Y = \begin{pmatrix} Y_1 & Y_2 & Y_3 & Y_4 \\ Y_2 & Y_1 & Y_4 & Y_3 \\ Y_3 & Y_4 & Y_1 & Y_2 \\ Y_4 & Y_3 & Y_2 & Y_1 \end{pmatrix} \qquad \textbf{Equation C-2}$$

In a meander structure, the coupling exists between adjacent parallel lines (line-1 and 2, line-2 and 3) and non-adjacent parallel lines (line-1 and 3) as well. In the admittance matrix model, these are simply regarded as coupled line pairs with different separations. The admittance elements for the adjacent coupled lines are labelled as Y_1 through Y_4 as given by (C-1), whereas only elements related to cross coupling are considered for the non-adjacent coupled lines. They are Y_3' and Y_4', given by

$$Y_3' = j\frac{1}{2}\left(Y_e'\csc(\theta_e') - Y_o'\csc(\theta_o')\right), \quad Y_4' = -j\frac{1}{2}\left(Y_e'\cot(\theta_e') - Y_o'\cot(\theta_o')\right) \qquad \textbf{Equation C-3}$$

The connections between the coupled line pairs are treated as single transmission lines, with a normalised admittance of $Y_s = Y_{s0}/Y_0$, a phase of $\theta_s = 2\pi f l_s/\upsilon_0$, and a velocity of $\upsilon_0 = c_0/\sqrt{\varepsilon_{eff}}$. The two independent matrix elements are the self-admittance

$$Y_{s1} = -jY_s\cot(\theta_s) \qquad \textbf{Equation C-4}$$

and the transmission-admittance

$$Y_{s2} = jY_s\csc(\theta_s) \qquad \textbf{Equation C-5}$$

All the normalised admittances, phases, and velocities are calculated using analytical formulas based on conformal mapping, as discussed in Appendix B.

The admittance matrix of the meander line contains both non-coupling-related elements and coupling-related elements. The non-coupling-related elements are the self-admittances (Y_1, Y_{s1}) and transmission-admittances (Y_2, Y_{s2}). The coupling-related elements are Y_3, Y_4, Y_3' and Y_4'. The Y-matrix of the 2-port 6-node meander line can be expressed as

$$Y_{6x6} = \begin{pmatrix} Y_1 & Y_2 & 0 & 0 & 0 & 0 \\ Y_2 & Y_1+Y_{s1} & Y_{s2} & 0 & 0 & 0 \\ 0 & Y_{s2} & Y_1+Y_{s1} & Y_2 & 0 & 0 \\ 0 & 0 & Y_2 & Y_1+Y_{s1} & Y_{s2} & 0 \\ 0 & 0 & 0 & Y_{s2} & Y_1+Y_{s1} & Y_2 \\ 0 & 0 & 0 & 0 & Y_2 & Y_1 \end{pmatrix} + \begin{pmatrix} 0 & 0 & Y_3 & Y_4 & Y_4' & Y_3' \\ 0 & 0 & Y_4 & Y_3 & Y_3' & Y_4' \\ Y_3 & Y_4 & 0 & 0 & Y_3 & Y_4 \\ Y_4 & Y_3 & 0 & 0 & Y_4 & Y_3 \\ Y_4' & Y_3' & Y_3 & Y_4 & 0 & 0 \\ Y_3' & Y_4' & Y_4 & Y_3 & 0 & 0 \end{pmatrix} \qquad \textbf{Equation C-6}$$

The first matrix contains the elements related to non-coupling contributions, the second contains those related to the coupling between both adjacent and non-adjacent lines. It should be noted that the self-admittance Y_{11} in the above matrix (Y_{11}=Y_1, Y_1 is defined in (C-1)) is slightly different from Swanson's general coupling model (GCM)[2] and Chen's multi-conductor model[3]. In Swanson's model, the self-admittance Y_{11} is assumed to be unaffected by the cross coupling. So, the self-admittance of a single line is used. That is

$$Y_{11} = -jY_s \cot(\theta) \qquad \textbf{Equation C-7}$$

In Chen's model, the cross-coupling effect on the self-admittance of the node in the *i*-th line is considered by

$$Y_{11} = Y_{11}^{(i)} + \sum_{j=1,\, j\neq i}^{n} \left(Y_{11}^{(i,j)} - Y_{11}^{(i)}\right) k_{ij}, \quad (\mathrm{i} = 1, 2, ..., \mathrm{n}), \; k_{ij} = \begin{cases} 1, & \text{for } |\mathrm{i} - \mathrm{j}| \leq \mathrm{M}; \\ 0, & \text{for } |\mathrm{i} - \mathrm{j}| > \mathrm{M}. \end{cases} \qquad \textbf{Equation C-8}$$

where the number *M* determines the cut-off distance of the cross coupling and *n* is the total number of parallel lines. $Y_{11}^{(i)}$ is the self-admittance of a single line (*i*-th line) in the form of (C-7). $Y_{11}^{(i,j)}$ is the self-admittance with cross-coupling present between the *i*-th and *j*-th lines. The treatment used here assumes that only the adjacent coupling affects the self-admittance. This means *M* equals 1. So

$$Y_{11} = Y_{11}^{(i)} + \left(Y_{11}^{(i,i+1)} - Y_{11}^{(i)}\right) = Y_{11}^{(i,i+1)} = Y_1, \quad (\mathrm{i} = 1, 2, 3) \qquad \textbf{Equation C-9}$$

To find the S parameters of the 2-port meander line, the 6×6 admittance matrix given by (C-6) should be reduced to 2×2, using an impedance-matrix approach. Firstly, the 6×6 admittance matrix is transformed into 6×6 impedance matrix by

$$Z = Y^{-1}. \qquad \textbf{Equation C-10}$$

Since the meander line is a 2-port network, only two external currents I_1 and I_6 are non-zero as in the following matrix form.

$$\begin{pmatrix} V_1 \\ V_2 \\ V_3 \\ V_4 \\ V_5 \\ V_6 \end{pmatrix} = \begin{pmatrix} Z_{11} & Z_{12} & \cdots & \cdots & Z_{15} & Z_{16} \\ Z_{21} & Z_{22} & \cdots & \cdots & Z_{25} & Z_{26} \\ \vdots & \vdots & \ddots & \iddots & \vdots & \vdots \\ \vdots & \vdots & \iddots & \ddots & \vdots & \vdots \\ Z_{51} & Z_{52} & \cdots & \cdots & Z_{55} & Z_{56} \\ Z_{61} & Z_{62} & \cdots & \cdots & Z_{65} & Z_{66} \end{pmatrix} \begin{pmatrix} I_1 \\ 0 \\ 0 \\ 0 \\ 0 \\ I_6 \end{pmatrix} \quad \textbf{Equation C-11}$$

So the Z matrix can be reduced to

$$Z_{r2} = \begin{pmatrix} Z_{11} & Z_{16} \\ Z_{61} & Z_{66} \end{pmatrix}, \quad \textbf{Equation C-12}$$

relating the voltages V_1 and V_6 to the currents I_1 and I_6 on the two ports (node-1 and node-6). The corresponding scattering matrix can be calculated by

$$S_{r2} = (U_2 + Y_{r2})^{-1} \cdot (U_2 - Y_{r2}), \quad \textbf{Equation C-13}$$

where U_2 is a unit matrix, and $Y_{r2}=Z_{r2}^{-1}$. S_{11} and S_{21} of the meander line are

$$S_{11} = 20 \cdot \log(|S_{r2,11}|), \; S_{21} = 20 \cdot \log(|S_{r2,21}|). \quad \textbf{Equation C-14}$$

Admittance matrix method is a fast approach to analyse a structure with multiple coupled lines. However, as it employs a network model rather than electromagnetic model, there are some limitations. First, the coupling-related admittances (Y_3, Y_4, Y_3', Y_4') for the adjacent or non-adjacent lines are obtained as if they are pairs of isolated coupled lines, although they are interconnected with each other through the short connection lines. Second, the corners in the bend structures are disregarded. In addition, the accuracy of this method may be lost as the coupled length is close to half of a wavelength according to [2].

[1] G. I. Zysman, A. K. Johnson, "Coupled transmission line networks in an inhomogeneous dielectric medium", *IEEE Trans. Microwave Theo. Tech.*, vol. 17, no. 10, pp. 753-759, Oct. 1969.
[2] D. G. Swanson, "A novel method for modeling coupling between several microstrip lines in MIC's and MMIC's", *IEEE Trans. Microwave Theo. Tech.*, vol. 39, no. 6, pp. 917-923, Jun. 1991.
[3] Z. Q. Chen, "Fast computation of multiple parameters of multiconductor coupled microstrip lines", *IEEE Trans. Microwave Theo. Tech.*, vol. 43, no. 6, pp. 1393-1395, Jun. 1995.

Appendix D Microwave cables and connectors

Microwave coaxial cables and connectors/adaptors are essential parts in the measurements of HTS delay lines. A coaxial cable itself is also a conventional transmission media for a delay line. Some general information about the cables used in this work is given. Table D-1 and Table D-2 summarises the typical mechanical and electrical parameters of different cables. Figure D.1 shows the comparison of their attenuations, which can be a reference as they are used as delay lines. The mateability issue among different connectors is also briefed.

D.1 Microwave Coaxial Cables

The attenuation, operational frequency range and packaging size (limited by the bending radius) are important parameters of microwave coaxial cables concerned here. There are several simple formulas for the coaxial cables. The impedance of the cable only depends on the ratio of the dielectric diameter *D* and the inner conductor diameter *d*.

$$Z_0 = \frac{60}{\sqrt{\varepsilon_r}} \ln \frac{D}{d} \qquad \textbf{Equation D-1}$$

The signal delay is

$$t = 3.33\sqrt{\varepsilon_r}\,(ns/m) \qquad \textbf{Equation D-2}$$

The maximum operation frequency is defined by

$$f_{cutoff} = \frac{2 \cdot c}{\pi\sqrt{\varepsilon_r}\,(D+d)}(Hz) \qquad \textbf{Equation D-3}$$

Above this frequency, higher order modes will occur.

Table D-1 Technical specifications of RG405 and RG402 semi-rigid cables approved by MIL C-17 standard. (Dielectric: PTFE; signal delay: 4.8 ns/m; operating temperature: -40°C to +125°C)

Type	RG402/U	RG405/U
Centre conductor diameter	0·92mm	0·51mm
Outer conductor diameter	3·58mm	2·20mm
Max. operating frequency	20GHz	20GHz
Attenuation (per 1m) at 1GHz	0·36dB	0·67dB
10GHz	1·37dB	2·43dB
20GHz	2·13dB	3·21dB
Weight	479g/m	202g/m

According to their formability, microwave coaxial cables can be classified into: semi-rigid, handformable and flexible.

Semi-rigid cable is also called form-stable cable, which can be bent to and then maintain the finished shape. The most used semi-rigid cables are RG405 and RG402. Their technical specifications are in Table D-1.

Handformable cable is an alternative to semi-rigid cable. They have a tin-soaked copper braid for the outer conductor, giving outstanding hand-formability. According to Huber+Suhner, the SUCOFORM-250 cable in this category is especially suitable for delay line due to the high phase stability over every production run.

Flexible microwave cable assemblies offer superior electrical and mechanical performance, where stringent electrical requirements - in particular stability and low loss - are important. This type of cable is ideally suited for test and measurement applications as test leads.

Parameters of several cables in these categories are listed in Table D-2. They are compiled from the product data of Huber+Suhner. Their attenuations as a function of frequency are fitted to the form

$$a\sqrt{f} + b \cdot f, \quad \text{(dB/m)} \qquad \textbf{Equation D-4}$$

The coefficient b is much smaller than a, so it is close to an $f^{0.5}$ relationship. The attenuations of different coaxial cables are plotted in Figure D.1. Generally, the attenuation is inversely proportional to the dimension d and D of the coaxial, so the thinner the cable is, the more loss it has.

Table D-2 Typical parameters of several microwave cables. (Source: http://www.hubersuhner.com)

Model[+]	Type	Max. freq. (GHz)	Temp. range (°C)	Attenu. (dB/m) @18GHz, 25°C	Delay (ns/m)	Static bending radius (mm)	Weight (kg/100 m)	Typical applications
EZ 250-TP/M17	Semi-rigid	18	-40 ~ +90	1.5	4.8	19.00	15.8	Static connections
EZ 118-TP	Semi-rigid	40	-40 ~ +125	1.8	4.17	9.53	3.4	
EZ141-TP/M17 (RG402)	Semi-rigid	20	-40 ~ +125	2.09	4.8	6.35	5.22	
SUCOFORM 250	Handformable	18	-65 ~ +165	1.45	4.7	30	12.4	Delay lines
SUCOFLEX 104	Flexible	26.5	-55 ~ +165	1.1	4.3	16	8.4	Test leads
SUCOFLEX 104P	High flexible	26.5	-55 ~ +165	1.6	4.3	16	6.9	Dynamic applications

[+] M17: MIL C-17 standard; TP: tin plated; AL: aluminium (If aluminum is used for the outer conductor, the weight and size could be reduced but it brings slightly higher loss).

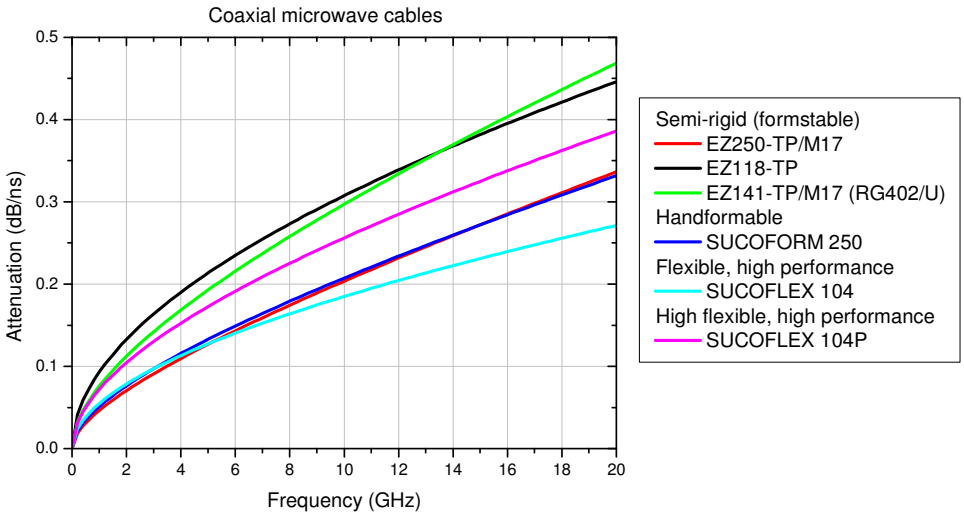

Figure D.1 Attenuation as a function of frequency for the coaxial cables listed in Table D-2.

The system for the cryogenic measurements in this thesis has semi-rigid RG405 and flexible SUCOFLEX 104. Semi-rigid cables are used as the connections inside the cryostat. They work at temperatures as low as 13K and in the vacuum. Although commercially available coaxial cables are not designed for the cryogenic conditions, experiences show that they can operate beyond the specified lower temperature limit (around -40 ^{o}C) without obvious problems. Flexible cables are used as connections between the network analyser and the cryostat. These cables offer high stability in terms of phase, attenuation and matching.

D.2 Connectors and Adaptors

In selecting the connectors/adaptors used in a microwave system, the most important criteria are the maximum operational frequency and their mateability with other connectors or adaptors. Table D-3 lists the mateability between three types of connectors. SMA is one of the most commonly used connectors. It has a PTFE dielectric. It is intended for infrequent connections. Unlike SMA, 3.5 mm and 2.92mm ("K") connectors have air as their dielectrics. They are connectors of higher performance, and can tolerate more interconnect cycles.

SMA can mate with 3.5mm and 2.92mm. But as they have different dielectric materials (PTFE versus air), their connection interface is discontinuous. There is also a problem of possible damaging when a male SMA is inserted into 3.5mm or 2.92mm connectors. This is

often caused by the pin of SMA, which is not well gauged. So, special care must be taken in connecting male SMA with 3.5mm or 2.92mm connectors.

In some circumstances, right-angle connectors or adaptors are needed to facilitate assembly. It should be noted that non-straight connectors normally have a lower operating frequency than their straight version in the same series. For instance, a right-angle SMA has a maximum operating frequency of 12.4 GHz rather than 18 GHz which is for a straight SMA.

Table D-3 Mateability among some microwave connectors.[1]

Connector Type	SMA[a]	3.5 mm[b]	2.92mm[c] & K[d]
SMA	To 18 GHz	To 18 GHz Usable to 24 GHz * Note: possible damage	To 18 GHz Usable to 24 GHz * Note: possible damage
3.5 mm	To 18 GHz Usable to 24 GHz * Note: possible damage	To 34 GHz	To 34 GHz
2.92 mm & K	To 18 GHz Usable to 24 GHz * Note: possible damage	To 34 GHz	To 46 GHz

Some manufacturers of the different type of connectors.
[a] M/A-COM SMA
[b] Agilent 3.5mm
[c] Pasternack 2.9mm
[d] Anritsu K-connector

[1] More information may be found from http://www.wa1mba.org/rfconn.htm.

Appendix E Attenuation calculated from resonator *Q* measurements of a delay line

Figure E.1 Equivalent circuit of a delay line resonator.

The deduction in this section was first proposed by Dr. F. Huang.[1] It is dedicated to study the effect of the dispersion on the acquisition of attenuation from measured *Q*, which has not been addressed before. The commonly used derivation in the textbook always assumes a dispersionless resonator.

As shown in Figure E.1, the input and output of the resonator are capacitively coupled to a delay line with a total length of *l*. The characteristic impedance of the delay line is the same as the port impedance in this derivation, which is Z_0. The propagation constant is γ. The loss of the delay line is assumed to be small, so that

$$\alpha l << 1, \text{ and } e^{\alpha l} \approx 1 + \alpha l .$$

This is a good approximation provided the frequency is not too high. The approximation $\sin(\beta l) << 1$ (in the proximity of a resonance peak) is used throughout the derivation.

The ABCD matrix of the delay line resonator is

$$\begin{bmatrix} A & B \\ C & D \end{bmatrix} = \begin{bmatrix} 1 & Z \\ 0 & 1 \end{bmatrix} \begin{bmatrix} t & Z_0 \cdot s \\ s/Z_0 & t \end{bmatrix} \begin{bmatrix} 1 & Z \\ 0 & 1 \end{bmatrix} = \begin{bmatrix} t + \dfrac{Z}{Z_0} s & 2Z \cdot t + \dfrac{Z^2}{Z_0} s + Z_0 \cdot s \\ \dfrac{s}{Z_0} & \dfrac{Z}{Z_0} s + t \end{bmatrix} \quad \text{Equation E-1}$$

where $Z = 1/(j\omega C), \quad t = \cosh(\gamma l), \quad s = \sinh(\gamma l)$.

From ABCD matrix, the insertion loss S_{21} can be found by

[1] F. Huang, private communication, EDT Group, EECE, The University of Birmingham, Notes, 16th Dec. 2003.

$$S_{21} = \frac{2}{A + B/Z_0 + CZ_0 + D} = \frac{2}{2(1 + Z/Z_0)e^{\gamma l} + (Z^2/Z_0^2)\sinh(\gamma l)}$$ **Equation E-2**

E.1 Weakly coupled resonator

If the resonator is weakly coupled at the input and output, $|Z|^2$ can be much larger than $|Z_0|^2$ so that one has

$$(Z^2/Z_0^2)\sinh(\gamma l) >> 2(1 + Z/Z_0)e^{\gamma l}$$ **Equation E-3**

which requires

$$\left|\frac{Z}{Z_0}\right|^2 \alpha l >> 2 \cdot \left|1 + \left(\frac{Z}{Z_0}\right)\right|$$

Since $|Z| >> |Z_0|$, one has $|Z/Z_0| \cdot \alpha l >> 2$.

In this case, the first term in the denominator of (E-2) can be dropped, so

$$S_{21} = \frac{2}{(Z^2/Z_0^2)\sinh(\gamma l)} = \frac{Z_0^2}{Z^2}\frac{4}{e^{\gamma l}(1 - e^{-2\gamma l})}$$ **Equation E-4**

The measurable resonance curve is the magnitude of S_{21} as a function of frequency, which can be written as

$$|S_{21}| = \frac{Z_0^2}{|Z|^2}\frac{4}{e^{\alpha l}|1 - e^{-2\gamma l}|} = \frac{Z_0^2}{|Z|^2}\frac{4}{e^{\alpha l}}\frac{1}{\sqrt{1 - 2e^{-2\alpha l}\cos(2\beta l) + e^{-4\alpha l}}}$$ **Equation E-5**

In the proximity of the resonance peak, the attenuation α and reactance Z are not sensitive to frequency. So it is $|1 - e^{-2\gamma l}|$ that contributes to the rapid change of S_{21} with frequency.

At the resonant frequency, let $\beta = \beta_n$ and $\omega = \omega_n$. $|S_{21}|$ gains the maximum, so

$$2\beta_n l = 2\pi n, \ (n = 1, 2, ...)$$ **Equation E-6**

Using $\alpha l << 1$, one has

$$\left|1-e^{-2\gamma l}\right|_{peak} = 1-e^{-2\alpha l} \approx 2\alpha l \qquad \textbf{Equation E-7}$$

To estimate the 3dB-Q, the 3dB bandwidth $\Delta\omega$ is needed. At the -3dB points, let $\beta = \beta_n + (\Delta\beta/2)$ and $\omega = \omega_n + (\Delta\omega/2)$, this gives

$$\begin{aligned}\left|1-e^{-2\gamma l}\right|_{-3dB} &= \left|1-e^{-2\alpha l}e^{-j2\beta_n l}e^{-j(\Delta\beta)l}\right| \\ &= \left|1-e^{-2\alpha l}e^{-j(\Delta\beta)l}\right| \\ &\approx \left|2\alpha l + j(\Delta\beta)l\right|\end{aligned} \qquad \textbf{Equation E-8}$$

Since $\left|S_{21}\right|_{-3dB} = \sqrt{0.5}\left|S_{21}\right|_{peak}$, by using (E-5), (E-7) and (E-8), one has

$$\begin{aligned}\frac{1}{\left|1-e^{-2\gamma l}\right|_{-3dB}} &= \frac{\sqrt{0.5}}{\left|1-e^{-2\gamma l}\right|_{peak}} \\ \frac{1}{\left|2\alpha l + j(\Delta\beta)l\right|} &= \frac{\sqrt{0.5}}{2\alpha l} \\ \alpha &= \Delta\beta/2\end{aligned} \qquad \textbf{Equation E-9}$$

Hence, the attenuation is correlated with the measured Q and group velocity v_g by

$$\begin{aligned}\alpha &= \frac{1}{2}\frac{\Delta\beta}{\Delta\omega}\frac{\Delta\omega}{\omega_n}\cdot 2\pi f_n \\ &= \pi\frac{1}{v_g}\frac{1}{Q_n}f_n \\ &= \frac{\pi}{Q_n\left(v_g/f_n\right)}\end{aligned} \qquad \textbf{Equation E-10}$$

For a dispersionless transmission-line resonator with $v_g = v_p$, (E-10) becomes the commonly used equation in textbooks[1]. That is

$$\alpha = \frac{\pi}{Q_n\left(v_p/f_n\right)} = \frac{\pi}{Q_n\lambda_n} \qquad \textbf{Equation E-11}$$

From the above deduction, it can be seen that (E-10) is the general form for an attenuation-Q relation, using the group velocity rather than phase velocity. This is particularly important as far as the dispersion is concerned. It should also be noted that Q_n in (E-10) and (E-11) approximates the unloaded Q_0, as a weak external coupling is assumed.

E.2 Strongly coupled resonator

If the external coupling is strong, (E-2) cannot be simplified to (E-4), instead

$$S_{21} = \frac{1}{e^{\gamma l}} \frac{4}{4(1+Z/Z_0)+\left(Z^2/Z_0^2\right)\left(1-e^{-2\gamma l}\right)} = \frac{1}{e^{\gamma l}}\left(\frac{Z_0}{Z}\right)^2 \frac{4}{\left[1+2(Z_0/Z)\right]^2 - e^{-2\gamma l}} \quad \textbf{Equation E-12}$$

$|Z|^2 >> |Z_0|^2$ is still assumed although (E-3) is no longer valid. Let

$$1+2(Z_0/Z) = \sqrt{r}e^{j\theta/2} \quad \textbf{Equation E-13}$$

where $r = 1+4\left|Z_0/Z\right|^2$, $\theta \approx 4\left|Z_0/Z\right|$ (since Z is imaginary and $|Z|^2 >> |Z_0|^2$).

The magnitude of S_{21} becomes

$$\left|S_{21}\right| = \frac{1}{\left|e^{\gamma l}\right|}\left|\frac{Z_0}{Z}\right|^2 \frac{4}{\left|re^{j\theta} - e^{-2\gamma l}\right|} \quad \textbf{Equation E-14}$$

A procedure similar to (E-6)~(E-10) is followed. At the resonant frequency,

$$2\beta_n l = 2\pi n + \theta \ (n=1, 2, \ldots) \quad \textbf{Equation E-15}$$

$$\left|re^{j\theta} - e^{-2\gamma l}\right|_{peak} \approx 4\left|Z_0/Z\right|^2 + 2\alpha l \quad \textbf{Equation E-16}$$

$$\left|S_{21}\right|_n \approx \frac{1}{e^{\alpha l}}\left|\frac{Z_0}{Z}\right|^2 \frac{4}{4\left|Z_0/Z\right|^2 + 2\alpha l} = \frac{1}{e^{\alpha l}} \frac{2}{2+\left|Z/Z_0\right|^2 \alpha l} \quad \textbf{Equation E-17}$$

Applying the approximation $\left|e^{\gamma l}\right| = e^{\alpha l} \approx 1+\alpha l$, one has

$$1-(1+\alpha l)\left|S_{21}\right|_n = \frac{\alpha l}{2\left|Z_0/Z\right|^2 + \alpha l} \quad \textbf{Equation E-18}$$

While at the -3dB points,

$$\left|re^{j\theta} - e^{-2\gamma l}\right|_{-3dB} \approx \left|4\left|\frac{Z_0}{Z}\right|^2 + 2\alpha l + j(\Delta\beta)l\right| \quad \textbf{Equation E-19}$$

A derivation similar to (E-8)~(E-10) leads to

$$\frac{\alpha}{1-(1+\alpha l)|S_{21}|_n} = \frac{\pi}{Q_n(v_g/f_n)}. \qquad \textbf{Equation E-20}$$

Here Q_n is the loaded (measured) quality factor and $|S_{21}|_n$ is the insertion loss at the n-th resonant frequency. For a symmetrically coupled resonator, the unloaded Q_0 can be expressed as

$$Q_0 = \frac{Q_n}{1-|S_{21}|_n} \qquad \textbf{Equation E-21}$$

If αl is much smaller than 1, (E-20) can be reduced to the same form as (E-10):

$$\alpha = \frac{\pi}{Q_0(v_g/f_n)} \qquad \textbf{Equation E-22}$$

If α is in the unit of dB/m rather than neper/m as in (E-22), a multiplicative factor 8.68 is needed, that is

$$\alpha = \frac{8.68\pi}{Q_0(v_g/f_n)} \qquad \textbf{Equation E-23}$$

[1] D. M. Pozar, *Microwave engineering*, Addison-Wesley, 1990, pp. 338.

Appendix F Fractal delay lines

F.1 Space-filling fractal structure

Among a large family of fractal structures, only the "space-filling curve" is considered here, as it can be easily adapted to a transmission line and makes a good use of substrate area. Figure F.1 (a) and (b) are two such fractal structures, with input/output lines added. Many more space-filling structures have been demonstrated in a book about space-filling curves[1]. This type of fractal structure is superior in its uniform routing density. Geometrically, it has a self-similarity[1] but no periodicity. For a microwave circuit, this is useful to eliminate the bandgap due to periodicity. Three space-filling curves are considered: Hilbert curve (Figure F.1(a)), Moore curve (Figure F.1(b)), and Peano curve (Figure F.4(a)). These curves can be mathematically produced using recursion process[1]. The iterations of the recursion determine the order of generation of a fractal structure, which is the number after the name, such as Hilbert-4. The total length of the structure increases exponentially with the order of generation. Several simulation examples are presented towards the application as delay lines.

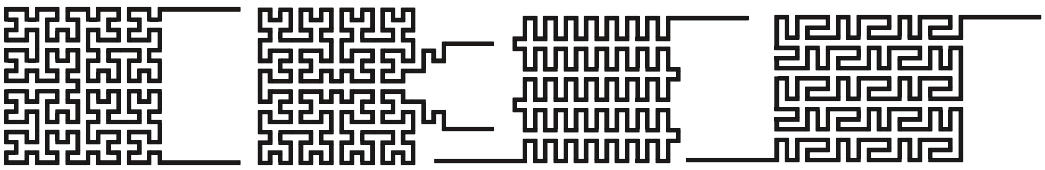

Figure F.1 Four microstrip-type layouts used in Sonnet simulations. The microstrip line width is 0.085 mm, the inter-line distance (centre to centre) is 0.255 mm, the gap between microstrip lines is 0.17 mm.

F.2 Fractal delay lines

Figure F.1 shows four microstrip layouts used in simulations. The first two are space-filling fractal structures. Figure F.1(d) is based on a Peano fractal, which is modified in order to match the length of the other 3 structures. Simulation results in Figure F.2 show that all four structures have transmission notches above 10 GHz.

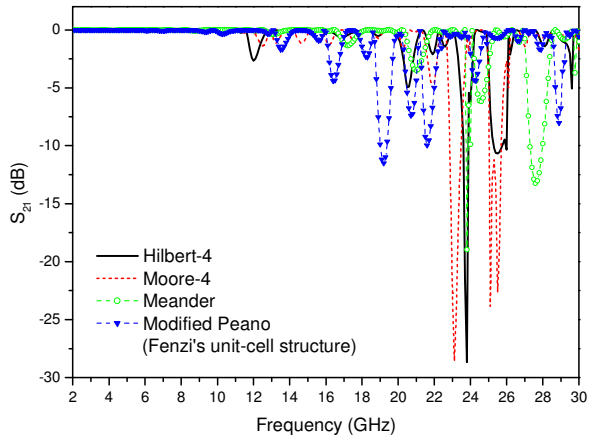

Figure F.2 Sonnet simulation results of the layouts shown in Figure F.1.

It is worth mentioning that Figure F.1(d) is similar to the structure used in Fenzi's HTS delay line[2] shown in Figure 2.6. Figure F.3 shows three microstrip lines with different routing structures, but all based on a unit-cell similar to Fenzi's delay line[2]. In Figure F.3, (A) is a Peano fractal, (B) is wound into a double spiral, and (C) is wound into a meander as Fenzi's delay line[2] does. Again, all have transmission notches above 10 GHz (Figure F.4). Among these three structures, the Peano-3 gives the best performance between 10 and 20 GHz.

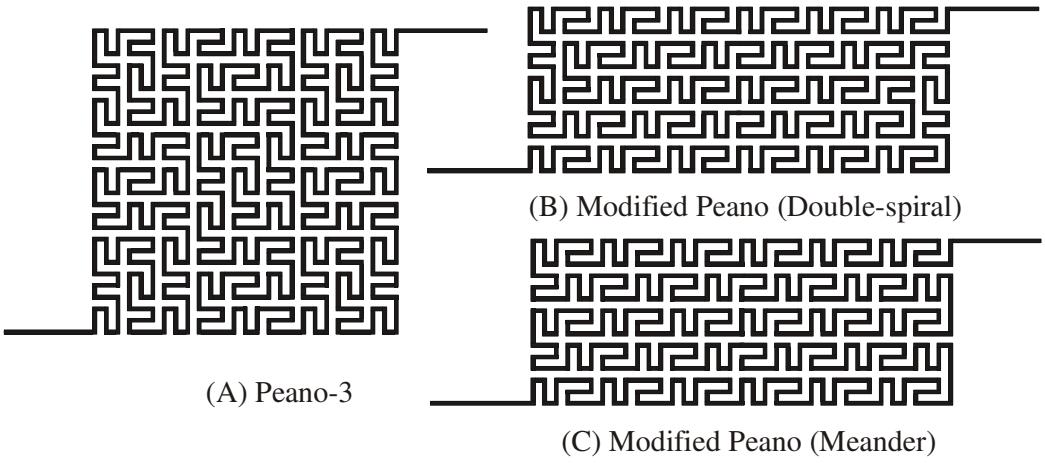

Figure F.3 Three microstrip lines with different routing structures but based on similar unit-cell. The microstrip line width is 0.085 mm, the inter-line distance is 0.255 mm, the gap between microstrip lines is 0.17 mm.

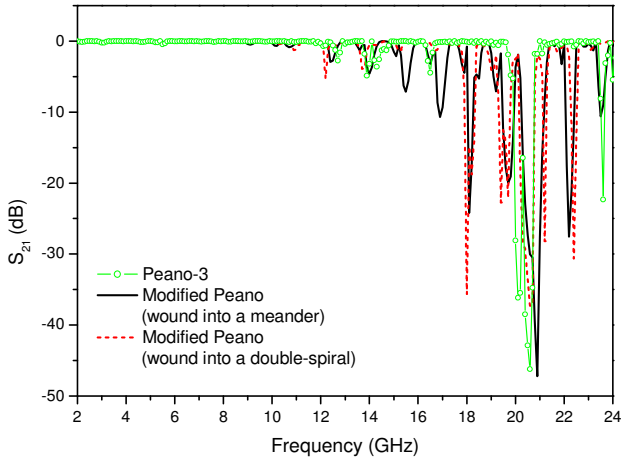

Figure F.4 Sonnet simulation results of the layouts shown in Figure F.3.

Coplanar-type fractal delay lines as shown in Figure F.5 are also simulated. In Figure F.6, each of the simulation results is compared with a microstrip line of the same structure and similar circuit size. Due to stronger cross coupling between microstrip lines, the microstrip structure has much wider transmission notches than the corresponding coplanar structure. For the CPW fractal line, highly uneven current distribution is observed on the in-plane grounds. It is believed that the in-plane grounds in fractal coplanar lines present particularly serious problem, as many of them are trapped in between the circuitous signal line without direct connections with the ground patch. Therefore, quarter-wavelength or half-wavelength resonances can be easily induced on the in-plane grounds. In addition, seen from Figure F.5(B), the in-plane grounds effectively turn into a patch network, which may cause some radiation loss.

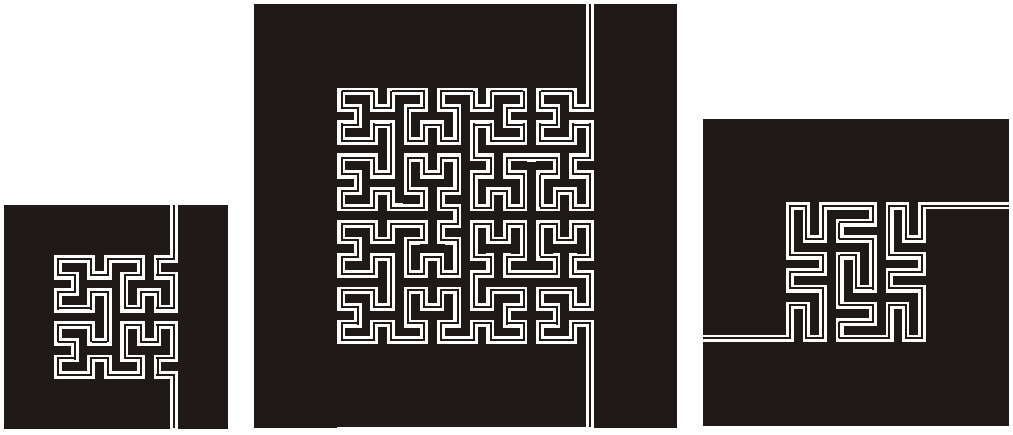

Figure F.5 Coplanar-type layouts with Hilbert-3, Hilbert-4, and Peano-2 structures.

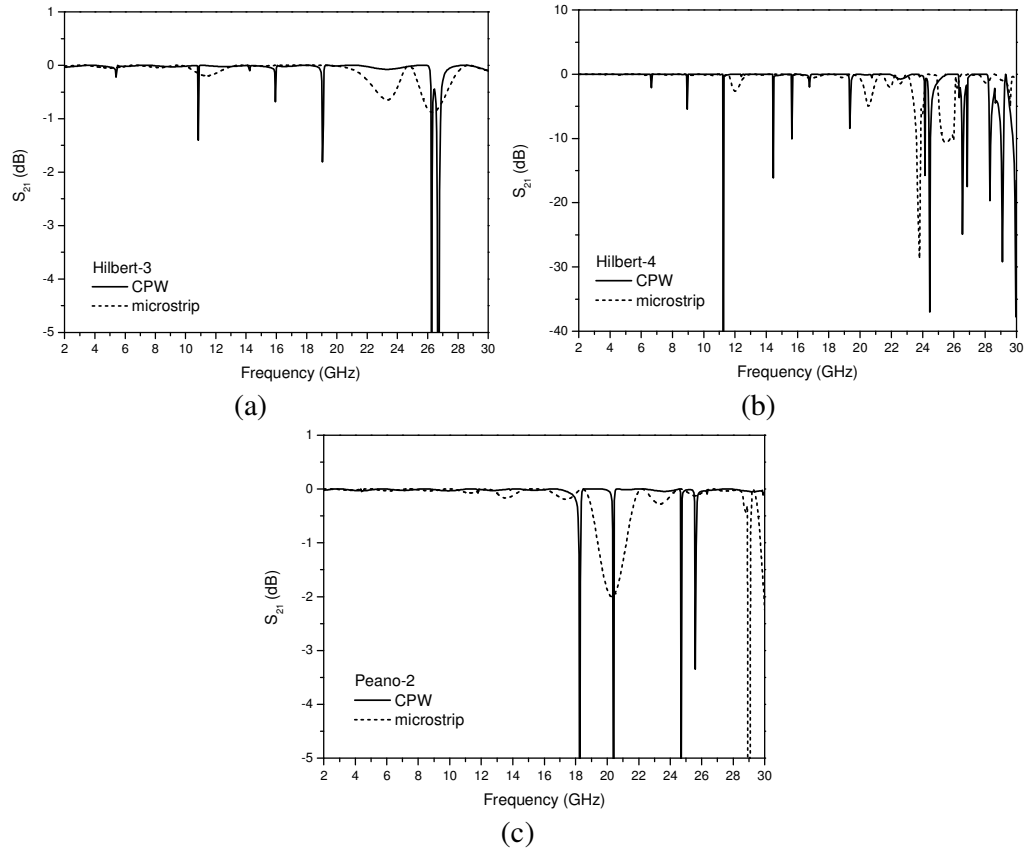

Figure F.6 Sonnet simulation results of (a) Hilbert-3, (b) Hilbert-4, and (c) Peano-2 structures of both coplanar-type (Figure F.5) and microstrip-type. The line width of the CPW is 0.02 mm, slot width is 0.04 mm, and the inter-line distance is 0.2 mm. The microstrip has the same dimensions as the layouts in Figure F.1. Excluding the in-plane ground patch, the CPW circuits occupy slightly smaller area than the microstrip ones of the same structure.

In summary, delay lines with space-filing fractal structures can have an efficient occupancy of the substrate area, with a uniform routing density. But the circuitous structure is an obstacle to achieving wide bandwidth. It is believed that more reflective resonances occur in fractal transmission lines due to the various bends. For a microstrip line, the coupling should be another concern. For a coplanar line, the unbalanced in-plane ground is a big problem. A large number of crossover interconnections may be needed in order to achieve a wide resonance-free passband.

[1] H. Sagan, *Space-filling curves*, New York: Springer-Verlag, 1994.
[2] N. Fenzi, D. Aidnik, D. Skoglund, S. Rohlfing, "Development of high temperature superconducting 100 nanosecond delay line", in *High-T_c microwave superconductors and applications*, Robert B. Hammond, Richard S. Withers, Editors, Proc. SPIE 2156, pp. 143-151, 1994.

Publications:

With major contribution,

[1] Y. Wang, H. T. Su, F. Huang, M. J. Lancaster, "Design of wideband superconducting coplanar delay lines", in *2003 High Frequency Postgraduate Student Colloquium*, pp 86-89, Sept. 2003.

[2] Y. Wang, F. Huang, M. J. Lancaster, H. T. Su, "Design considerations of coplanar-to-coaxial transitions for wideband HTS delay lines," in *34th European microwave conference*, pp. 177-180, Oct. 2004.

[3] Y. Wang, H. T. Su, F. Huang, M. J. Lancaster, "Wideband superconducting coplanar delay lines", *IEEE Trans. Microwave Theory Tech.*, accepted for publication, July 2005.

With partial contribution,

[4] H. T. Su, Y. Wang, F. Huang, M. J. Lancaster, "Characterizing a Double-Spiralled Meander Superconducting Microstrip Delay Line using a Resonator Technique", in *2004 IEEE MTT-S International Microwave Symposium*, vol. 1, no. 1, pp. 135-138, 2004.

[5] H. T. Su, Y. Wang, F. Huang, M. J. Lancaster, "Wideband superconducting microstrip delay line", *IEEE Trans. Microwave Theory Tech.*, vol. 52, no. 11, pp. 2482-2487, Nov. 2004.

Publication plan:

With major contribution

Y. Wang, H. T. Su, F. Huang, M. J. Lancaster, "Measurement of Surface Resistance for YBCO Thin Film Using Coplanar Line Resonator Techniques from 20 MHz to 20 GHz", to be submitted to *IEEE Trans. Applied Superconductivity*.

With partial contribution

H. T. Su, Y. Wang, F. Huang, M. J. Lancaster, "Superconducting Delay Lines", review paper, to be submitted to *Superconductor Science and Technology*, in preparation.